Optica Applicata, Vol. XLIII, No. 2, 2013
DOI: 10.5277/oa130218

Optimized three-step phase-shifting profilometry using the third harmonic injection

CHAO ZUO[1, 2*], QIAN CHEN[1, 2], GUOHUA GU[1], JIANLE REN[1], XIUBAO SUI[1], YUZHEN ZHANG[1]

[1]Jiangsu Key Laboratory of Spectral Imaging and Intelligence Sense,
Nanjing University of Science and Technology, Nanjing, Jiangsu Province 210094, China

[2]Key Laboratory of Photoelectronic Imaging Technology and System,
Ministry of Education of China, Beijing Institute of Technology, Beijing 100081, China

[*]Corresponding author: surpasszuo@163.com

Three-step phase-shifting is an extensively employed method for three-dimensional (3D) shape measurement, especially for high speed 3D image acquisition. However, since only three fringe images are used, the measurement result is susceptible to sensor and environment noise. In this paper, we propose a third harmonic injection technique for three-step phase-shifting profilometry to reduce the error caused by the uncertainty noise. By adding a measure of third harmonic to the sinusoidal waveform, the amplitude of the sinusoidal foundational component can be increased by 15.5%, which results in the reduction of the phase error caused by random noise. The advantages of the proposed technique lie in its simplicity, insensitivity to image defocus, and applicability for high speed 3D imaging by projector defocus. Theoretical analysis, simulations, and experiments are presented to verify the effectiveness of the proposed technique.

Keywords: three-dimensional shape measurement, phase-shifting, harmonic injection.

1. Introduction

Fringe projection profilometry (FPP) is one of the leading optical metrological tools for three-dimensional (3D) shape extraction. Because of its numerous advantages, such as non-contact, high accuracy, low cost and high flexibility, FPP has been widely used in such fields as computer-aided design and manufacturing, reverse engineering, rapid prototyping, and 3D virtual reality [1–4]. The fundamental principle of FPP is that periodic fringe patterns are projected on the measured object, and the distorted patterns caused by the depth variation of the surface are recorded from different directions. The phase distributions of the distorted fringe patterns are often recovered by phase-shifting techniques, and then the depth map of the object surface is further reconstructed. However in practice, there are many factors such as nonlinear response of the projector, camera noise, projector noise, and ambient light noise affecting the measurement accuracy of a 3D shape measurement system [5–10].

Many studies have been performed on the effects of projector nonlinearity and a variety of techniques have been proposed with this purpose [7, 8]. In contrast, the ef-

fects of random noise are trickier since the error introduced is phase independent. To reduce the effects of noise on the resulting 3D surface reconstructions, JIELIN LI *et al*. [9] proposed a white-noise model for phase-shifting profilometry that they then applied to optimize a two-frequency phase measurement technique. YONGCHANG WANG *et al*. [10] proposed an edge pattern strategy to increase the signal-to-noise ratio (SNR) of patterns by maximizing the computational length. However, this technique is sensitive to image defocus and resolution difference between the projector and the camera.

In order to minimize total scan time to reach real-time 3D measurements, three-step phase-shifting algorithm are typically used to reconstruct a single 3D shape [5, 6]. However, since only three fringe patterns are used, the measurement accuracy is very sensitive to the system noise. Therefore, in this paper, we focus our attention on reducing the impact of random noise in three-step phase-shifting algorithm. We found that to reduce the error standard deviation of calculated phase in the three-step phase-shifting, the only way is to increase the amplitude of the sinusoidal pattern. But the amplitude of the sinusoidal pattern is limited by the dynamic range of the projector and the sensitivity of the camera which are difficult to improve. By regarding the triplen harmonics are eliminated from the phase in the three-step phase-shifting, we can add triplen harmonics to the original sine waveform without changing the calculated phase. We further derived that, by adding a measure of third harmonic to the sine waveform, it is possible to obtain 15.55% higher effective amplitude of the fundamental signal. In this way, the error standard deviation of the calculated phase in the three-step phase-shifting can be reduced accordingly. Besides, our technique is insensitive to image defocus and easy to be generated by a binary pattern with project defocus, which is favorable for high speed, real-time 3D imaging.

This paper is organized as follows. In Section 2, the three-step phase-shifting algorithm is briefly recalled, and the mathematical analysis of the effect of noise on the reconstructed phase is given. In Section 3, the proposed third harmonic injection technique is described in detail. The simulation and experimental results are presented in Sections 4 and 5. Finally, the conclusions of the paper are summarized in Section 6.

2. Effect of noise on the three-step phase-shifting algorithm

2.1. Three-step phase-shifting algorithm

As introduced above, the three-step phase-shifting algorithm requires minimum number of fringe images to reconstruct 3D shape. Thus it is usually used for time--critical applications. In general, the three encoded fringe images $\{I_i: i = 1, 2, 3\}$ in project space (x^p, y^p) with a phase shift of $2\pi/3$ generated by a computer are:

$$I_i(x^p, y^p) = A + B\cos\left(\phi(x^p) - \frac{2\pi i}{3}\right) \tag{1}$$

where A is the temporal DC value, and B is the amplitude (or projector modulation) of the temporal AC signal; $\phi(x^p)$ is the phase information and is designed according to $2\pi F/W$, where W is the pattern width and F is the total number of periods for one

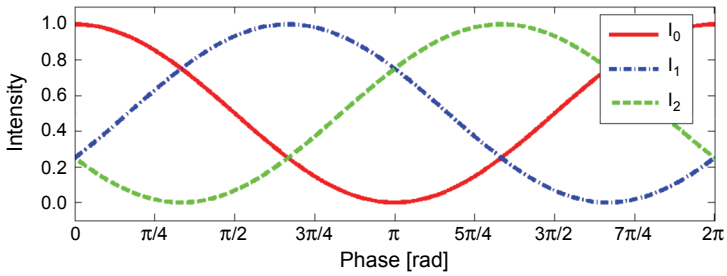

Fig. 1. Cross-sections of the three phase-shifted sinusoidal fringe patterns.

row. Without loss of generality, we assume that the fringes are perpendicular to the x^p-axis in this paper. To make full use of the entire dynamic range of the projector [0, 1], A and B are normally both 0.5. The cross-sections of the three fringe images are illustrated in Fig. 1.

After projecting the patterns to the object, the reflection process captured by a camera can be expressed as:

$$I_i(x, y) = \alpha(x, y)\left[A + B\cos\left(\phi(x, y) - \frac{2\pi i}{3}\right) + \beta(x, y)\right] \tag{2}$$

where (x, y) is the camera coordinate, $\alpha(x, y)$ represents the albedo within [0, 1] while 0 is pure black and 1 is pure white; $\beta(x, y)$ represents the ambient illumination; $\phi(x, y)$ is the desired phase information. For simplicity, $I_i(x, y)$ is commonly denoted as

$$I_i(x, y) = a(x, y) + b(x, y)\cos\left(\phi(x, y) - \frac{2\pi i}{3}\right) \tag{3}$$

where $a(x, y)$ is average intensity which equals $\alpha(x, y)[A + \beta(x, y)]$, $b(x, y)$ is the intensity modulation which equals $\alpha(x, y)B$. The desired phase information can be solved from these equations,

$$\phi(x, y) = \tan^{-1}\left\{\frac{\sqrt{3}\left[I_2(x, y) - I_3(x, y)\right]}{2I_1(x, y) - I_2(x, y) - I_3(x, y)}\right\} \tag{4}$$

The extracted phases have principle values ranging for $-\pi$ and $+\pi$. It needs phase unwrapping process to recover the absolute phase. After the phase unwrapping process is carried out to obtain the continuous natural phase distribution, the phase map can be further converted to 3D coordinate values with calibration and a phase-coordinate conversion algorithm [2].

2.2. Influence of noise on the calculated phase

During the actual phase calculation process, the captured fringe images are contaminated by intensity noise. The noise sources include ambient light, shadowing,

projector illumination noise, camera/projector flicker, camera noise, and quantization error in the frame grabber and the projector. To simplify our analysis, we assume that the combination of noise is additive, white, Gaussian random variable $n_i \sim N(0, \sigma_n)$, and by adding the noise, the captured images $I_i'(x, y)$ can be rewritten as:

$$I_i'(x, y) = I_i(x, y) + n_i(x, y) \tag{5}$$

Therefore, the measured phase can be calculated by substituting Eq. (5) into Eq. (1) as follows:

$$\phi'(x, y) = \tan^{-1}\left\{ \frac{N_1 + 3b(x, y)\sin\left[\phi(x, y)\right]}{N_2 + 3b(x, y)\cos\left[\phi(x, y)\right]} \right\} \tag{6}$$

where $N_1 = \sqrt{3}(n_2 - n_3)$ and $N_2 = 2n_1 - n_2 - n_3$. Auxiliary variables N_1 and N_2 are also Gaussian, *i.e.*, $N_1 \sim N(0, 6\sigma_n^2)$ and $N_2 \sim N(0, 6\sigma_n^2)$. The measured phase can be considered as the sum of the actual phase and the phase error caused by the noise. Thus, we have

$$\Delta\phi(x, y) = \phi'(x, y) - \phi(x, y) = \\ = \tan^{-1}\left\{ \frac{N_1\cos\left[\phi(x, y)\right] - N_2\sin\left[\phi(x, y)\right]}{N_1\sin\left[\phi(x, y)\right] + N_2\cos\left[\phi(x, y)\right] + 3b(x, y)} \right\} \tag{7}$$

Because the noise is usually much smaller than the intensity modulation $b(x, y)$, we can further approximate Eq. (7) to

$$\Delta\phi(x, y) \approx \frac{N_1\cos\left[\phi(x, y)\right] - N_2\sin\left[\phi(x, y)\right]}{3b(x, y)} \tag{8}$$

To measure how the noise will affect the phase calculated, the phase error variance is calculated as [6]

$$\sigma_{\Delta\phi}^2(x, y) \approx \frac{6\sigma_n^2\left\{\cos^2\left[\phi(x, y)\right] + \sin^2\left[\phi(x, y)\right]\right\}}{9b^2(x, y)} = \frac{2}{3}\left[\frac{\sigma_n}{b(x, y)}\right]^2 \tag{9}$$

From Equation (9), we can see the phase error standard deviation $\sigma_{\Delta\phi}(x, y)$ is proportional to the intensity noise σ_n and inversely proportional to $b(x, y)$, the intensity modulation. It can be further noted that $b(x, y) = \alpha(x, y)B$, where $\alpha(x, y)$ is a reflection

constant which is only related to the object of interest. Therefore, the only way to reduce the phase error in the three-step phase-shifting method is to increase B. However, it is commonly accepted that B is limited by the system setup and difficult to improve [9].

3. Third harmonic injection technique

From above analysis, we know for a three-step phase-shifting pattern strategy, the optimization of patterns is achieved by maximizing the amplitude of the sinusoidal foundational component B. Besides, we hope the optimization of the pattern should have the following basic properties:

1. The modification of waveform should not affect the phase value in order to achieve an accurate 3D reconstruction based on phase.

2. The pattern should have excellent resistance to errors caused by image defocusing since the measured object may cover a large depth range.

3. It is better that the pattern is easy to be generated and could be realized by binary pattern with camera defocus.

We first focus on the first two properties. With the satisfaction of the property 1, the optimized pattern should not change the phase calculated by Eq. (4). In order to satisfy property 2, the spectrum of the pattern should be less shaper, *i.e.*, containing less high-order harmonics which may be sensitive to the projector defocusing. For example, the sinusoidal pattern is insensitive to defocusing since its spectrum contains only one principle frequency component. The defocusing effect can be modeled as the convolution of a sharp image with the point spread function (PSF). The PSF is usually approximated by a circular Gaussian function. The Gaussian low-pass filter will attenuate the magnitude of frequency component, but the sinusoidality of the pattern is unchanged so that no phase error will be induced. Therefore, it is best that changing the amplitudes of different harmonics components of the spectrum of the pattern does not affect the calculated phase.

3.1. Cancellation of triplen harmonics in the three-step phase-shifting method

For the three-step phase-shifting method, if third harmonics are contained in the fringe patterns, *i.e.*, the captured images are composed of the fundamentals plus an arbitrary amount of any third harmonics, there is:

$$I_i''(x,y) = a(x,y) + b(x,y)\cos\left[\phi(x,y) - \frac{2\pi i}{3}\right] + \\ + c(x,y)\cos\left\{3\left[\phi(x,y) + \Delta\theta - \frac{2\pi i}{3}\right]\right\} \tag{10}$$

The wrapped phase is still obtained by using Eq. (4)

$$\phi''(x,y) = \tan^{-1}\left\{\frac{\sqrt{3}\left[I_2''(x,y) - I_3''(x,y)\right]}{2I_1''(x,y) - I_2''(x,y) - I_3''(x,y)}\right\} = \phi(x,y) \tag{11}$$

It is shown that the third harmonics in the fringe patterns are cophasal and are therefore canceled during the phase calculation. This means the existence of the third harmonics does not induce any phase errors for three-step phase-shifting algorithm. To find all the error-free harmonics and give a more understandable demonstration of why these harmonics can be canceled in the three-step phase-shifting algorithm, we explain this point using the frequency transfer function (FTF) theory detailed in [11]. The phase-shifting algorithms can be viewed as complex quadrature filters in the temporal domain. Specifically, for three-step phase-shifting we can revise Eq. (3) as

$$I_i(x,y) = a(x,y) + \frac{b(x,y)}{2}\exp\left\{-i\left[\phi(x,y) - \frac{2\pi i}{3}\right]\right\} + \\ + \frac{b(x,y)}{2}\exp\left\{i\left[\phi(x,y) - \frac{2\pi i}{3}\right]\right\} \tag{12}$$

The aim of the three-step phase-shifting algorithm is to filter out the average intensity $a(x,y)$, and one of the two complex exponentials so that the desired phase information can be extracted. If we represent the three-step phase-shifting algorithm as a temporal filter, its frequency transfer function (FTF) $H(\omega)$ can be written as:

$$H(\omega) = \left[1 - \exp\left(i\frac{2}{3}\pi\omega\right)\right]\left[1 - \exp\left(i\frac{2}{3}\pi(\omega+1)\right)\right] \tag{13}$$

Figure 2 presents the magnitude of $H(\omega)$ in the range of [–9, 9], from which it can be seen that the $H(0) = 0$, $H(-1) = 0$ and $H(1) = 3$. This is expected since it guarantees that the two unwanted terms in Eq. (12) can be filtered out. More importantly, we can see that the FTF of the three-step phase-shifting algorithm has zeroes at ±3, ±6, ±9....

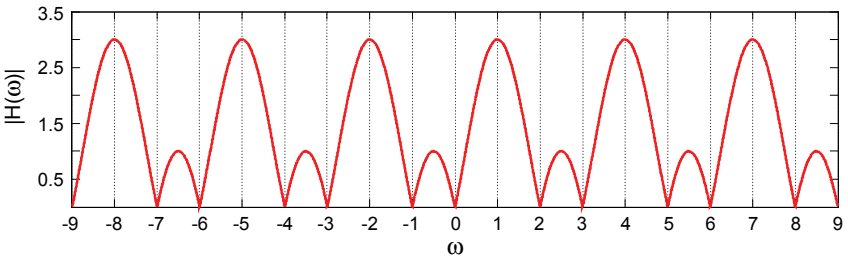

Fig. 2. Spectral magnitude of the three-step phase-shifting algorithm in Eq. (4).

Therefore, we can readily understand that the three-step phase-shifting algorithm is insensitive to triplen harmonics.

Although the triplen harmonics are eliminated from the phase, they could decrease the peak of the sinusoidal waveforms, thus it allows the dynamic range of resulting waveform further being amplified. In this way, the phase error can be reduced without changing the original algorithm. Besides, image defocus will not cause errors in the presence of triplen harmonics. When the image is defocused, the amplitude of different frequency components of the pattern may be attenuated, especially for the high order triplen harmonic components. But it does not introduce any phase error, only the contrast of the pattern may be decreased.

3.2. Calculation of optimum distortion

To obtain the best modification of the waveforms, the optimum amplitude of the triplen harmonics should be derived. The best modification should be made to decrease the peak-to-peak amplitude of the original sinusoidal waveform by the greatest extent. Then the dynamic range of the pattern is reduced while the effective amplitude of the sinusoidal component is unchanged. In another word, the dynamic range of the pattern can be further boosted with the effective amplitude of the sinusoidal component increased.

We first *only* add a measure of the third harmonic and derive the optimal parameters. Then it will be subsequently shown that *no further improvement* can be derived from the addition of other triplen harmonics. Without loss of the generality, we assume a one dimensional phase waveform of the type

$$I = \cos(\theta) + C\cos\left[3(\theta + \Delta\theta)\right] \tag{14}$$

where $\Delta\theta$ is the phase deviation, C is the amplitude parameter. Obviously, to reduce the peaks of the sinusoidal waveform most effectively, the optimal value of the phase deviation $\Delta\theta$ should be zero and C should be negative so that the valleys of the triplen harmonics could be directed toward the peaks of the sinusoidal waveform. Then the phase waveform can been written as

$$I = \cos(\theta) + C\cos(3\theta) \tag{15}$$

So we only need to determine the amplitude parameter C. We first locate the turning points of this function by differentiating I with respect to θ and equating the result to zero

$$\frac{\mathrm{d}I}{\mathrm{d}\theta} = -\sin(\theta) - 3C\sin(3\theta) = 0 \tag{16}$$

From the relation that $\sin(3\theta) = -4\sin^3(\theta) + 3\sin(\theta)$, we have $\sin(\theta) = 0$ or $\sin(\theta) = \pm\sqrt{(9C-1)/12C}$. Thus we have $\cos(\theta) = \pm 1$ or $\cos(\theta) = \pm\sqrt{(1+3C)/12C}$.

Considering the symmetry property of the waveform, we only take the positive solutions. The peak value of I can be found by substituting the two values of $\cos(\theta)$ obtained into Eq. (15), and using the identity $\cos(3\theta) = 4\cos^3(\theta) - 3\cos(\theta)$, we have the two peak value of I:

$$\hat{I} = 1 + C \tag{17}$$

or

$$\hat{I} = 8C\left(\frac{3C-1}{12C}\right)^{3/2} \tag{18}$$

The optimum value for C is that value which minimizes the value of $\hat{I}$. It can therefore be found by differentiating the expression for C and equating the result to zeros. Since the differentiation of Eq. (17) with respect to C is always 1, it cannot be used to decide the optimal value of C. Thus we only use Eq. (16):

$$\frac{\mathrm{d}\hat{I}}{\mathrm{d}C} = \left(\frac{3C-1}{12C}\right)^{1/2}\left(2 + \frac{1}{3C}\right) = 0 \tag{19}$$

from which we obtain $a = 1/3$ or $-1/6$. Disregarding the positive solution, we have the optimum value for a is $-1/6$, and the required waveform is

$$I = \cos(\theta) + \frac{1}{6}\cos(3\theta) \tag{20}$$

Further, it can be also derived that no further reduction in $\hat{I}$ is possible by the addition of other triplen harmonics, since the maximum of $\hat{I}$ is got at $\theta = \pi/3$ or $2\pi/3$ and all triplen harmonics pass through zero at these values of 0. We now substitute the value of $\theta = \pi/3$ in Eq. (20), and we obtain the peak values of $\hat{I}$. Hence

$$\hat{I} = \pm\frac{\sqrt{3}}{2} = \pm 0.866 \tag{21}$$

As has been shown, the addition of one-sixth of third harmonic to the modulating waveform has the effect of reducing the peak value of the output waveform by a factor

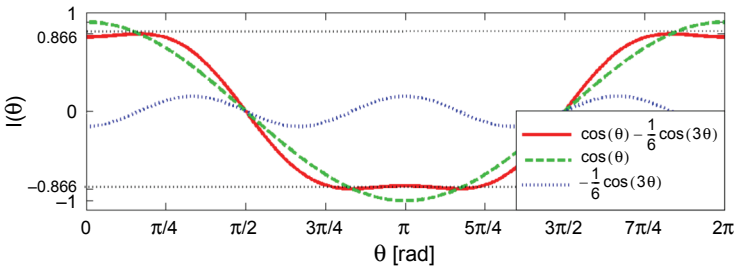

Fig. 3. Reduction of peak value by adding one-sixth of third harmonic. Peak value of the resultant waveform is 0.866, the amplitude of the fundamental is 1.

of 0.866 without changing the amplitude of the fundamental. This process is illustrated in Fig. 3. It is then possible to increase the amplitude of the modulating wave by a factor K so that the full dynamic range of the projector is again utilized. Thus the modulating waveform becomes

$$I = K\left(\cos(\theta) + \frac{1}{6}\cos(3\theta)\right) \tag{22}$$

From Equation (21) we know that the previous peak value of I was 0.866. Therefore, we have

$$K = \frac{1}{0.866} = 1.155 \tag{23}$$

The analytical expression for the reference waveform is

$$I = 1.155\cos(\theta) - 0.192\cos(3\theta) \tag{24}$$

Thus as Fig. 4 shows, the addition of one-sixth of third harmonic produces a 15.55% increase in the amplitude of the fundamental of the phase waveform and, therefore, the intensity noise σ_n can be decreased with the calculated phase unchanged.

3.3. Third harmonic injection with the pulse-width modulation technique

Through the addition of the 17% third-harmonic component to the original sine reference waveform, the resulting flat-topped waveform (Fig. 4) allows 15.55% improvement of the amplitude of the fundamental of the phase waveform with respect to the original one. This technique does not introduce any distortion to the phase value and is insensitive to image defocus. So the properties 1 and 2 are well satisfied.

In the above derivation, we assume that the relationship between the input gray-scale values and the gray-scale captured by the camera is linear. However, the gamma curve of the projector is usually not linear which will result in errors in the final measurement results. Recently, techniques concerning the use of binary patterns to generate sinusoidal fringe patterns by properly defocusing the projector are

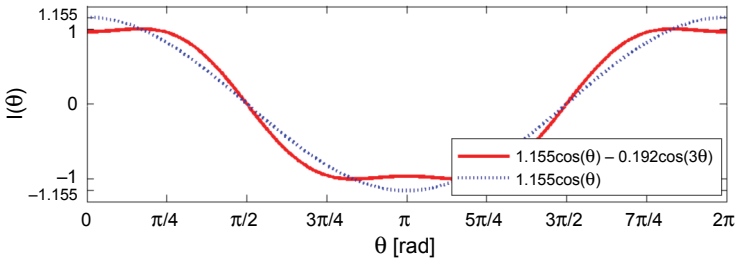

Fig. 4. Increasing the fundamental amplitude by restoring the peak value to one. The amplitude of the fundamental is 1.155.

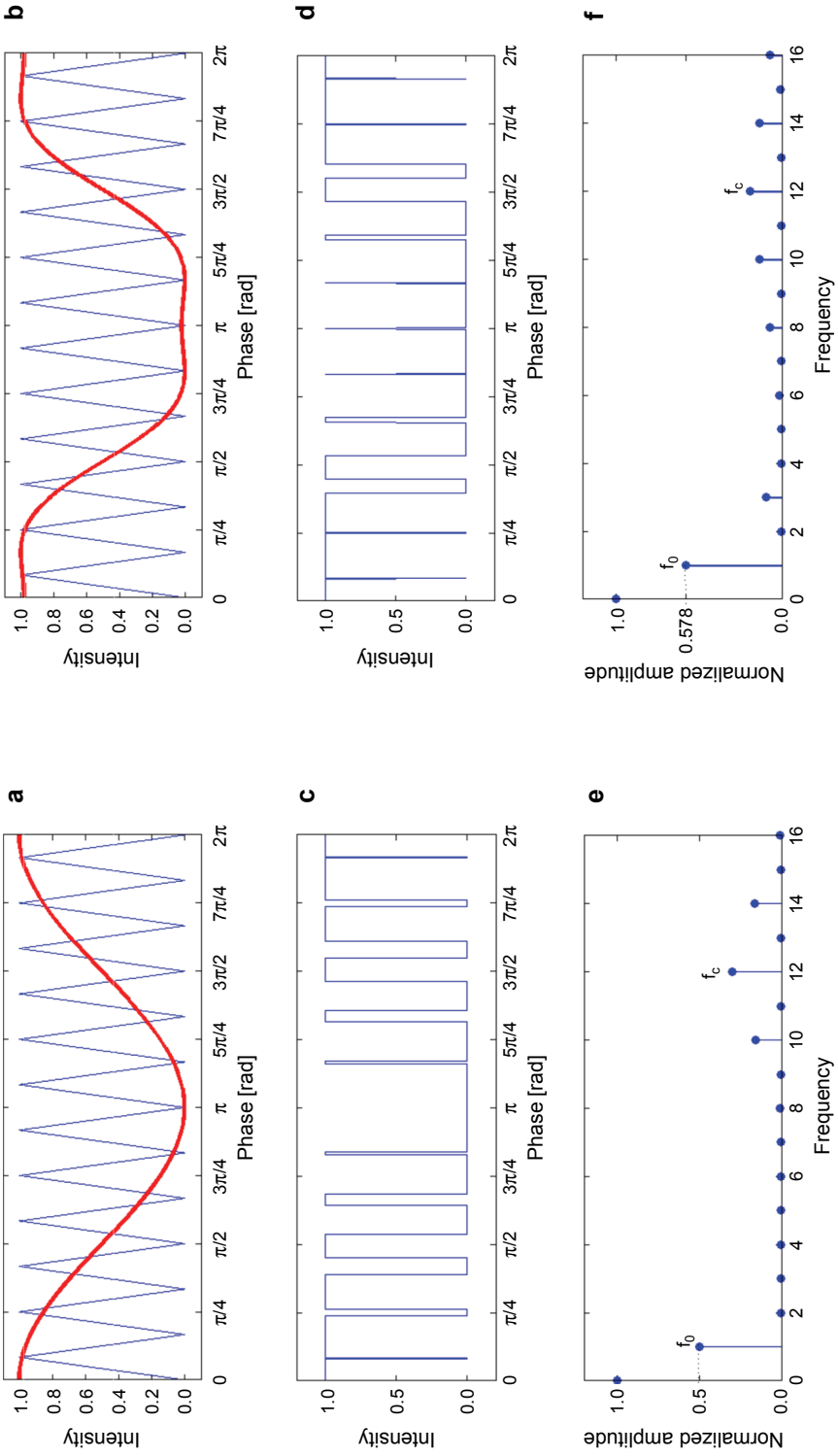

Fig. 5. Sinusoidal PWM (left) and third harmonic injection PWM (right). Original waveforms and the triangular carriers ($f_c = 12f_0$) are shown in (**a**) and (**b**). The corresponding PWM waveform is shown in (**c**) and (**d**). (**e**) and (**f**) show the spectrum of (**c**) and (**d**), respectively.

proposed [12–14]. These methods elude the nonlinearity problem effectively and are very useful for high speed measurement due to the operation mechanism of a digital micromirror device (DMD) in a DLP projector. That is the reason why we introduce the property 3. However, these methods are usually accompanied with the contrast reduction in fringe patterns as an undesired collateral effect.

Pulse-width modulation (PWM) technique is proposed in [14] to generate the high--quality sinusoidal pattern with a small defocusing level. Figure 5 gives an example to better illustrate its principle. The output binary patterns are modulated by comparing the desired sinusoidal pattern with a high-frequency triangular carrier. In the spectrum of the PWM pattern, the high-frequency harmonics are shifted farther away from the fundamental frequency and thus are easier to be suppressed by a low-pass filter. However, it also should be noticed that since the amplitude of the sinusoidal pattern could never be larger than that of the carrier, so the maximal normalized amplitude of the desired sinusoidal of frequency f_0 is 0.5. In practice, this value will be even less than this due to the defocus effect and the discrete nature of the generated fringe.

Our technique can also work well with the PWM technique. In Figure 5, it can be seen that, by adding the third harmonics into the original sinusoidal pattern, the peak of the original waveform is reduced by 15%, which allows a higher modulation index. Figure 5**f** gives the spectrum of the PWM pattern of the modified waveform, the amplitude of the desired sinusoidal of frequency f_0 is increased to 0.578. This means an improvement in the effective contrast of the sinusoidal pattern. It can also be noted that two high-frequency harmonics components at $f_c - 2f_0$ and $f_c + 2f_0$ crops up. However, they are easy to be suppressed by a small level defocus. Besides we seldom observe harmonic waves larger than fifth-order in the FPP system. Nevertheless, the amplitude of high-frequency harmonics at f is relatively high, so we recommended the use of $f_c = 12f_0$ to further suppress the 12th-order harmonics since the three-step phase-shifting method is insensitive to the 12th-order harmonics.

4. Simulation

Simulations were performed to verify the performance of the proposed method. In this simulation, we compare the accuracy of the traditional three-step phase-shifting method with the proposed third harmonic injection method. We assume that the project is perfectly linear and properly focused. Thus the phase error is due to the random noise only. The noise of the whole system is simulated by use of a zero-mean Gaussian random variable with a standard deviation of one.

An irregular surface is generated as the original phase distribution is shown in Fig. 6. In this simulation, all the images have 512×512 pixels of 256 gray levels. The simulated phase values are obtained by using Eq. (4), and the phase error is determined by comparing against the phase result from ideal fringe patterns which are free from the noise. A reference sinusoidal fringe pattern corresponding to a planar surface was simulated in Fig. 7**a**. By adding one-sixth of third harmonic and then increasing the amplitude of the modulating wave by 15.5%, we got the distorted fringe

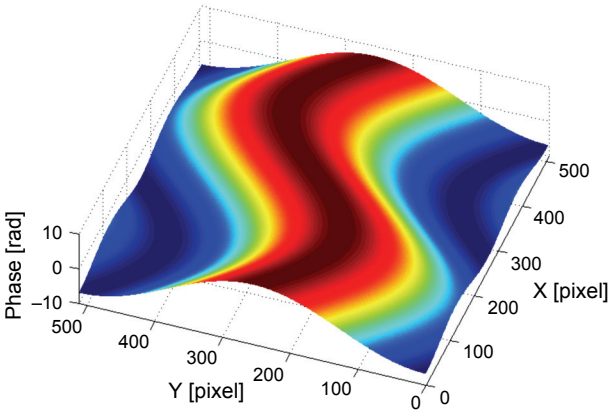

Fig. 6. The simulated phase map.

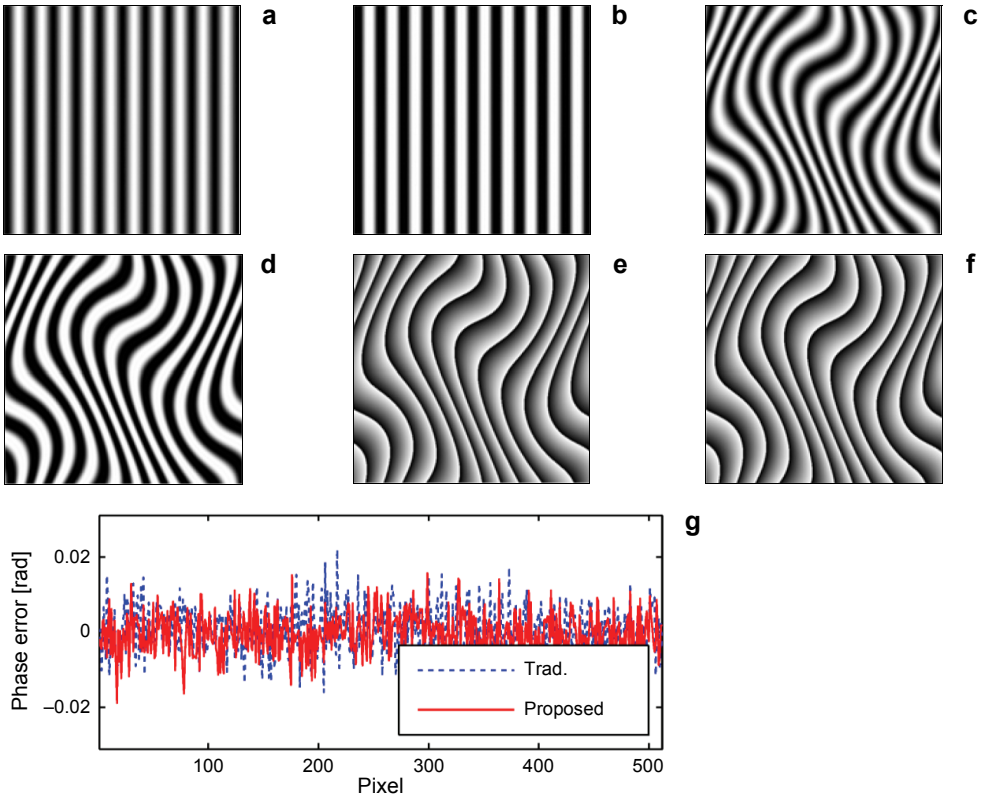

Fig. 7. Simulation results for the traditional three-step phase-shifting method (**a**, **c**, **e**) and the proposed third harmonic injection method (**b**, **d**, **f**). The reference fringe patterns of the two methods are shown in (**a**) and (**b**). (**c**) and (**d**) show the modulated patterns by the phase map shown in Fig. 6. The warped phase is shown in (**e**) and (**f**) and the cross-sections of the phase error are shown in (**g**).

pattern shown in Fig. 7**b**. The fringe modulated patterns by the phase distribution are shown in Figs. 7**c** and 7**d**. The estimated phase by using the two fringe patterns are shown in Figs. 7**e** and 7**f**, respectively.

To better illustrate, the cross-section comparison of the phase error using two tested patterns are shown in Fig. 7**g**. It can be seen that, by applying the third harmonics injection technique, our technique gives a more accurate result than that of the traditional method. Further, to accurately quantify the differences between the two methods, the simulation is repeated for 500 times to get the standard deviation of the phase error. Results show that, by using the proposed third harmonics injection method, the standard deviation value of the calculated phase error is reduced from 0.0107 to 0.0089. This simulation confirmed that our technique could increase the SNR of the acquired patterns and reduce the phase error caused by the sensor noise by about 15% without any changes in algorithm, which agrees well with the prediction of Eq. (9).

5. Experiment results

Fringe projection experiments are conducted to test the practical applicability of the proposed method. An DLP projector Acer X1261 is used as a structured light source. The deformed fringe patterns are captured by a CCD camera JAI CA-M50 and are digitized by an 8-bit frame grabber card. The procedure of generation, projection, recording and processing of the fringe patterns was automated using the *Image Acquisition Toolbox* of MATLAB. Four different fringe patterns are generated for comparison: focused sinusoidal pattern, focused distorted sinusoidal pattern by third harmonic injection, defocused sinusoidal PWM patterns, and defocused distorted sinusoidal by third harmonic injection PWM patterns. The recorded fringe pattern images corresponding to a uniform flat surface using different methods are shown in Figs. 8**a**–8**d**. Figures 8**e**–8**h** show the corresponding intensity cuts across the patterns. As a comparison, if the camera is in focus, the fringe images have higher contrast. However, the patterns suffer from the error which results from the nonlinearity of the gamma of the projector. When the projector is defocused and the PWM technique is applied to the sinusoidal wave, the fringe contrast is reduced, but the sinusoidality of the waveform is significantly improved. Similarly, the third harmonic distorted sinusoidal pattern can be also obtained free of nonlinearity by using the modulated binary pattern under a low defocusing level. Compared with defocused sinusoidal PWM pattern, it has higher effective contrast.

We also measured a plaster head model. One recorded fringe pattern modulated by the 3D sculpture surface profile is shown in Fig. 9**a**. Figures 9**b**–9**e** show the measurement results corresponding to four different methods. For the results using the focused fringe patterns (Figs. 9**b** and 9**c**), the reconstructed surface profiles are superimposed by a spurious periodic undulation, which are due to the nonlinear response of the projector. Compared with the phase error introduced by the camera

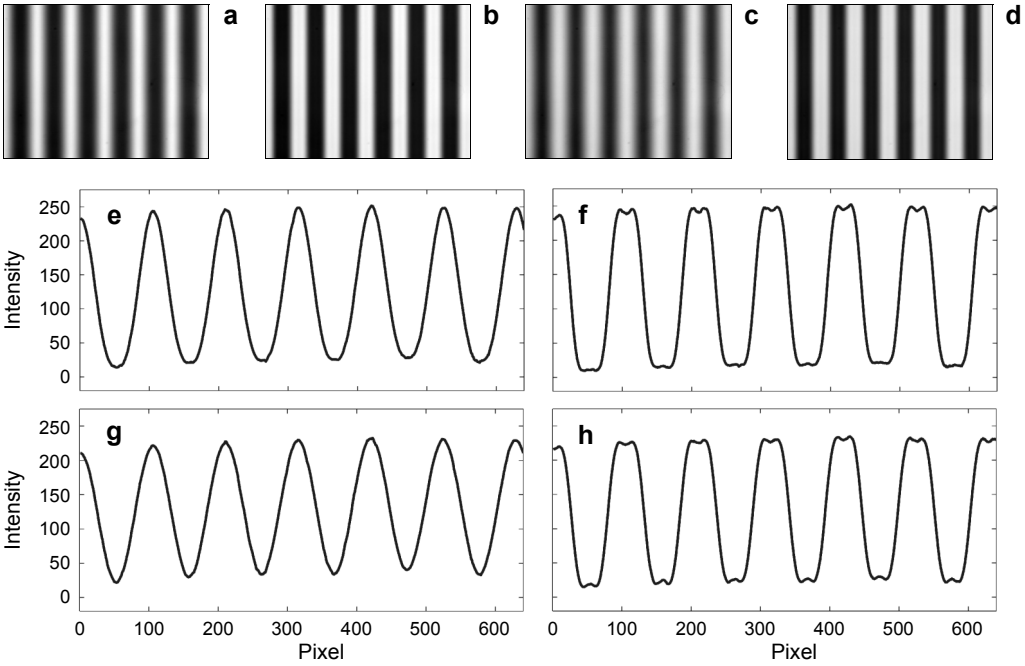

Fig. 8. Captured fringe images for focused sinusoidal pattern (**a**), focused distorted sinusoidal pattern by third harmonic injection (**b**), defocused sinusoidal PWM pattern (**c**), and defocused distorted sinusoidal by third harmonic injection PWM pattern (**d**). (**e**)–(**f**) are the corresponding intensity cuts cross-sections of the four captured fringe images.

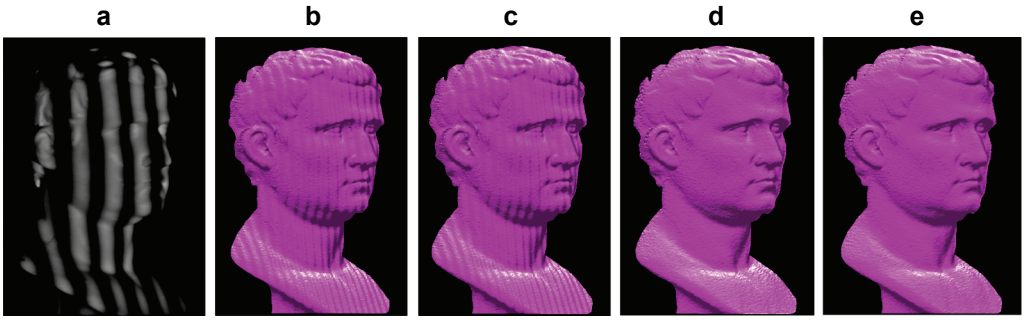

Fig. 9. Experimental results of a complex sculpture for both methods with different methods: one captured fringe image of measured human sculpture (**a**), result with focused sinusoidal patterns (**b**), focused distorted sinusoidal patterns by third harmonic injection (**c**), defocused sinusoidal PWM patterns (**d**), and defocused distorted sinusoidal by third harmonic injection PWM patterns (**e**).

noise, the error caused by the projector nonlinearity is much larger. So the former two methods give a similar quality of measurement. However, when the defocused fringe patterns are used, the periodic errors are reduced to a negligible level, because only two gray-scale values (0's and 255's) are used. Furthermore, it can be seen that the reconstructed 3D human face by using the third harmonic injection PWM patterns

is smoother than results using defocused sinusoidal PWM patterns. The results clearly prove the correctness of our theoretical analysis and the validity of the proposed method.

6. Conclusions

In this paper, we proposed a third harmonic injection technique for three-step phase shifting profilometry to reduce the error caused by the uncertainty noise. We have mathematically derived the effect of noise on the reconstructed phase error, and shown that in order to reduce the phase error, the only way is to increase the amplitude of the sinusoidal pattern. By regarding that the triplen harmonics are eliminated from the phase, it is possible to increase the amplitude of the sinusoidal foundational component by adding a measure of third harmonic to the original waveform. The maximal improvement in amplitude of the foundational component is obtained when the amplitude of the third harmonic is one-sixth of the fundamental one. Thus the phase error caused by noise can be reduced accordingly. Besides, the modified pattern is very easy to generate and insensitive to the error caused by image defocus without the need for changing the decoding algorithm. We further demonstrate that our technique can work well with the PWM technique, resulting in a contrast improvement in the generated pattern compared with the sinusoidal PWM method. These advantages make our method more desirable in accurate, high-speed 3D shape measurement.

Acknowledgements – This work was supported by the Research and Innovation Plan for Graduate Students of Jiangsu Higher Education Institutions, China (Grant No. CXZZ11_0237).

References

[1] SALVI J., PAGES J., BATLLE J., *Pattern codification strategies in structured light systems*, Pattern Recognition **37**(4), 2004, pp. 827–849.

[2] CHEN S.Y., LI Y.F., ZHANG J.W., *Vision processing for realtime 3-D data acquisition based on coded structured light*, IEEE Transactions on Image Processing **17**(2), 2008, pp. 167–176.

[3] SCHREIBER H., BRUNING J.H., *Phase shifting interferometry*, [In] *Optical Shop Testing*, 3rd Ed., D. Malacara [Ed.], Wiley, 2007, Chap. 14.

[4] RUSINKIEWICZ S., HALL-HOLT O., LEVOY M., *Real-time 3D model acquisition*, ACM Transactions on Graphics **21**(3), 2002, pp. 438–446.

[5] SONG ZHANG, VAN DER WEIDE D., OLIVER J., *Superfast phase-shifting method for 3-D shape measurement*, Optics Express **18**(9), 2010, pp. 9684–9689.

[6] CHAO ZUO, QIAN CHEN, GUOHUA GU, SHIJIE FENG, FANGXIAOYU FENG, *High-speed three-dimensional profilometry for multiple objects with complex shapes*, Optics Express **20**(17), 2012, pp. 19493–19510.

[7] HONGWEI GUO, HAITAO HE, MINGYI CHEN, *Gamma correction for digital fringe projection profilometry*, Applied Optics **43**(14), 2004, pp. 2906–2914.

[8] BING PAN, QIAN KEMAO, LEI HUANG, ANAND ASUNDI, *Phase error analysis and compensation for nonsinusoidal waveforms in phase-shifting digital fringe projection profilometry*, Optics Letters **34**(4), 2009, pp. 416–418.

[9] JIELIN LI, HASSEBROOK L.G., CHUN GUAN, *Optimized two-frequency phase-measuring-profilometry light-sensor temporal-noise sensitivity*, Journal of the Optical Society of America A **20**(1), 2003, pp. 106–115.

[10] YONGCHANG WANG, KAI LIU, LAU D.L., QI HAO, HASSEBROOK L.G., *Maximum SNR pattern strategy for phase shifting methods in structured light illumination*, Journal of the Optical Society of America A **27**(9), 2010, pp. 1962–1971.

[11] SERVIN M., ESTRADA J.C., QUIROGA J.A., *The general theory of phase shifting algorithms*, Optics Express **17**(24), 2009, pp. 21867–21881.

[12] CHAO ZUO, QIAN CHEN, SHIJIE FENG, FANGXIAOYU FENG, GUOHUA GU, XIUBAO SUI, *Optimized pulse width modulation pattern strategy for three-dimensional profilometry with projector defocusing*, Applied Optics **51**(19), 2012, pp. 4477–4490.

[13] SHUANGYAN LEI, SONG ZHANG, *Flexible 3-D shape measurement using projector defocusing*, Optics Letters **34**(20), 2009, pp. 3080–3082.

[14] AYUBI G.A., AYUBI J.A., DI MARTINO J.M., FERRARI J.A., *Pulse-width modulation in defocused three-dimensional fringe projection*, Optics Letters **35**(21), 2010, pp. 3682–3684.

Received January 18, 2012
in revised form August 14, 2012